

EXTENSION OF THE MATHEMATICAL ABSORBER REFLECTION SUPPRESSION TECHNIQUE TO THE PLANAR NEAR-FIELD GEOMETRY

Stuart Gregson, Allen Newell, Greg Hindman, Michael Carey
Nearfield Systems Inc.
19730 Magellan Drive,
Torrance, CA 90502-1104

ABSTRACT

Obtaining a quantitative accuracy qualification is one of the primary concerns for any measurement technique [1, 2]. This is especially true for the case of near-field antenna measurements as these techniques consist of a significant degree of mathematical analysis. When undertaking this sort of examination, room scattering is typically found to be one of the most significant contributors to the overall error budget [1]. Previously, a technique named Mathematical Absorber Reflection Suppression (MARS) has been used with considerable success in quantifying and subsequently suppressing range multi-path effects in first spherical [3, 4] and then, cylindrical near-field antenna measurement systems [5, 6]. This paper details a recent advance that, for the first time, enables the MARS technique to be successfully deployed to correct data taken using planar near-field antenna measurement systems. This paper provides an overview of the measurement and novel data transformation and post-processing chain. Preliminary results of computational electromagnetic simulation and actual range measurements are presented and discussed that illustrate the success of the technique.

Keywords: Near-Field, Antenna Measurements, Reflection Suppression, Planar MARS.

1. Introduction

Since its inception, the planar near-field (PNF) antenna measurement technique has developed into a powerful method for accurately and precisely characterising the performance of medium to high gain antennas at reduced range lengths [7]. Due to the finite size of the planar sampling interval and thus the necessity to characterise primarily directional antennas, range multi-path effects have typically been considered to be of lesser importance in planar than cylindrical or spherical measurement techniques. Clearly, the directional nature of the test antenna results in the region of greatest field intensities being concentrated on the parts of the chamber situated immediately behind the scan plane. As a result of cost considerations, it has become widespread practice to concentrate the placement of absorbent material around

the scanner leaving, in some cases, much of the remainder of the chamber uncovered. Thus, in some circumstances multiple-reflections within the chamber can become significant, *e.g.* when measuring lower gain antennas, wide out sidelobes, or low cross-polar patterns. Furthermore, any absorber which is used can not be perfectly matched to illuminating fields for all directions, polarisations and frequencies. Thus in some cases, the resulting scattering can impede the measurements taken therein. Whilst considerable effort, ingenuity and resourcefulness have been devoted to quantifying and subsequently improving the quality of multi-path contaminated measurements taken in spherical near-field (SNF), far-field, compact antenna test ranges (CATR), and cylindrical near-field (CNF) facilities, planar near-field (PNF) systems have received far less attention. Although aperture plane spatial filtering techniques have been proposed, the mode filtering techniques that have proved so overwhelmingly successful in spherical [3, 4] and cylindrical [5, 6] ranges have not previously been extended to the planar case.

The planar methodology requires that far-field antenna parameters such as pattern, gain, directivity, polarisation, *etc.*, be derived analytically from measurements taken in the near-field of a radiator. For such parameters, which can not be obtained directly from measurements made in the near-field, a transformation from one surface to another is necessitated. This transformation, of monochromatic but otherwise arbitrary waves, can be accomplished by representing the field at an arbitrary point in space as a summation of any elementary wave solutions to Maxwell's equations. Here, the mode coefficients to these solutions are determined by matching the fields over the surface on which the fields are known and by using mode orthogonality. Solving this modal expansion for the fields over the surface of a sphere with an infinite radius centred about the AUT results in the far-field pattern. A degree of mathematical convenience can be obtained from selecting a modal basis that is commensurate with the measurement geometry, *i.e.* by utilising plane waves, cylindrical waves, or spherical waves respectively for the case where the measurements are taken over planar, cylindrical or spherical surfaces. However, outside of the excluded regions, and as a consequence of the uniqueness principle, it is possible to equate the fields and thus express one mode set in terms

of another [8]. Here, the excluded region is that portion of space for which the spherical, cylindrical or planar expansions are *not* valid. For the spherical case this corresponds to a spherical volume that is centred about the origin of the measurement co-ordinate system that has a radius large enough to enclose the majority of the current sources. For the cylindrical cases the excluded region corresponds (analogously) to a right cylinder of infinite length that is centred about the origin of the measurement co-ordinate system that again has a radius large enough to enclose the majority of the current sources. Conversely for the planar case, it corresponds to the half-space that contains the radiator. Whilst the mode sets can be equated in almost any homogeneous linear isotropic source or sink free region of non-excluded space, by virtue of the simplification afforded by the commonality of co-ordinate system and polarisation bases, it is perhaps most convenient to equate electric or magnetic far-fields. As near-field measurements are taken outside the reactive near-field region, and as such evanescent fields are not sampled, choosing the far-field for this transformation of mode bases imposes no additional assumptions, approximations or limitations. It is therefore possible to obtain cylindrical and/or spherical mode coefficients from planar near-field measurements thereby extending the possibility of applying the highly sophisticated and well developed, mode spectrum filtering techniques directly to the planar near-field methodology. This is a very attractive proposition as the success of such measurement and mode filtering techniques has been attested to across a wide range of frequencies, on numerous different antenna measurement systems and antenna types.

2. Extension Of The MARS Principle To The Planar Near-Field Geometry

The general mathematical absorber reflection suppression (MARS) principle comprises a measurement and post-processing technique that analyses the measured data before utilising a filtering process to suppress undesirable scattered fields. This frequency-domain technique is completely general requiring only a minimum amount of information about the AUT and measurement configuration. The technique is entirely generic in nature and can be applied to a variety of different antenna types, *i.e.* no specific a priori assumptions about the arrangement of current sources are made. Thus, this technique is equally applicable to aperture, and *non*-aperture type antennas. However, it is assumed that the near-field antenna pattern function is spatially band-limited (*i.e.* the current sources occupy a finite region of space) and that the multiple reflections, arising from the various scatterers within the chamber are outside this region of space.

Generally when characterising an antenna it is installed within the system such that the majority of the current sources are situated about the origin of the range measurement co-ordinate system so that it is displaced in space as little as possible during the course of a measurement. As range multi-path tends to disturb the fields illuminating the test antenna, the purpose of this strategy is to insure that the field illuminating the test antenna vary as little as possible over the AUT during the course of the acquisition. However, the MARS measurement technique adopts a fundamentally opposing strategy whereby the test antenna is deliberately displaced from the centre of rotation. This has the effect of making the differences in the illuminating field far more pronounced than would otherwise be the case, and it is exactly this greater differentiation that makes their identification and subsequent extraction feasible. It has been found that the larger the displacement the more effective the filtering becomes. That is, until the separation is larger than the maximum dimension of the AUT whereupon the benefits of an increased separation can become negated by the increase in measurement time, the greater constraints of facility alignment, and in the cylindrical case unnecessary additional truncation.

For both the spherical and cylindrical implementations of MARS (S-MARS and C-MARS respectively), once the probe corrected far electric fields have been determined using standard probe-corrected near-field theory, the AUT is mathematically translated to the origin of the measurement frame of reference through the application of a differential phase change [5, 9], *i.e.*,

$$\underline{E}_i(r \rightarrow \infty, \theta, \phi) = \underline{E}(r \rightarrow \infty, \theta, \phi) e^{jk_0 \underline{r}} \quad (1)$$

Here, \underline{r} denotes the displacement vector between the centre of the measurement co-ordinate system and the centre of the current sources *e.g.* the aperture of the AUT. This has the corresponding effect of reducing the number of mode coefficients, either spherical or cylindrical, that are required to represent the radiated field. That is, we have reduced the MRE to a conceptual (*i.e.* optimised) minimum value allowing all higher order modes to be filtered out using a simple filter function without compromising the integrity of the underlying antenna pattern function. As usual, the magnitude of the MRE is determined by the physical size of the AUT. Furthermore, the act of displacing the AUT has the additional benefit of separating, *i.e.* orthogonalising, those modes associated with the AUT from those modes associated with a scatterer. Thus, in order to be able to extend the existing MARS methodology, two issues must be resolved. Firstly, how to obtain the mode coefficients from the planar near-field measurement and secondly, how to displace the AUT from the “centre of rotation” when seemingly there is no antenna rotation per say.

These questions are addressed and resolved in the following sections.

In principle, it is possible to obtain spherical mode coefficients (SMC) or cylindrical mode coefficients (CMC) from the plane wave spectrum (PWS). However, due to their greater numerical stability and the enormous ease and efficiency with which they can be obtained from far electric fields, it is perhaps preferable to work with CMCs. It is well known that it is possible to obtain probe pattern corrected far-fields directly from planar near-field measurements on an azimuth over elevation co-ordinate system by carefully selecting the direction cosines [9]. The angular spectrum can be obtained directly from the sampled tangential near-field components using,

$$\underline{E}_T(k_x, k_y, z=0) = \int_{-\infty}^{\infty} \int_{-\infty}^{\infty} \underline{E}_T(x, y, z=0) e^{j(k_x x + k_y y)} dx dy \quad (2)$$

Here, \underline{E}_T denotes the two tangential orthogonal sampled near-field components, $k_x = k_0 \sin A \cos E$, $k_y = k_0 \sin E$, $k_z = k_0 \cos A \cos E$ where A and E are used to denote the azimuth and elevation angles respectively, and k_0 is the free space propagation constant. In practice, this can be evaluated efficiently without recourse to approximation by implementing the two-dimensional integration as a series of y -axis one-dimensional integrations, before integrating this result as a series of one-dimensional x -axis integrals. Generally the measured spectral components are corrected for the directive and polarisation properties of the near-field probe. Probe pattern correction is not the subject of this paper and a detailed discussion can be found in the open literature, *e.g.* [7, 9] and its omission from this discussion is not a limitation of the technique. The propagating far electric field can be obtained from the tangential angular spectra using the method of stationary phase and the plane wave condition [9],

$$\underline{E}(k_x, k_y) \approx j \frac{e^{-jk_0 r}}{\lambda r} \frac{k_z}{k_0} \left[\underline{E}_T(k_x, k_y) - \frac{k_T \cdot \underline{E}_T(k_x, k_y)}{k_z} \hat{e}_z \right] \quad (3)$$

As all three Cartesian components of the far electric field are known, it is a trivial matter to resolve these fields onto a Ludwig II azimuth over elevation polarisation basis [9]. An azimuth over elevation system has been chosen since it has been shown previously that the equivalent cylindrical mode coefficients can be obtained from this data through the evaluation of [5, 6],

$$B_n^1(\gamma) = -\frac{(-j)^n}{4\pi\kappa} \int_0^{2\pi} E_A(r \rightarrow \infty, A, E) e^{-jnA} dA \quad (4)$$

$$B_n^2(\gamma) = j \frac{(-j)^n}{4\pi\kappa} \int_0^{2\pi} E_E(r \rightarrow \infty, A, E) e^{-jnA} dA \quad (5)$$

Here, a factor of 2π has been introduced in the denominator in (4, 5) to preserve the correct normalisation of the CMCs. Thus, it is possible to obtain CMCs from a planar-near field measurement without approximation. It is worth highlighting that there is a

difference in the suppressed time dependence between equations (2, 3) and (4, 5). If this difference is not accounted for correctly it has the principle effect of mapping n to $-n$. CMCs are complex numbers that are functions of the polarization index s , the ϕ index n and the Fourier variable γ . Figure 1 below contains a false colour checkerboard plot of the amplitudes of the CMCs modes for $s = 1$, *i.e.* B^1 , from a planar measurement of an x -band standard gain horn (SGH), *c.f.* Figure 14 below. From inspection of Figure 1 it can be seen that there are significant amounts of power distributed across a wide range of CMCs. However, it is clear that there is very little power contained in modes outside the $n^2 + (\gamma a)^2$ circle where a represents half the scan width of the planar near-field measurement. It is worth stating explicitly that this effect was *not* imposed by any conscious filtering of the CMCs, but rather is a natural consequence of the measurement process itself. Thus the larger the planar sampling interval, the higher the order of CMC that can be reconstructed from that data set. Here, $n_{\max} = k_0 a = 398$.

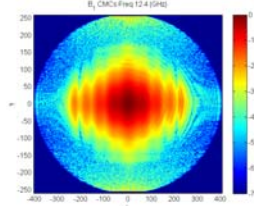


Figure 1 – CMCs Calculated from planar measurement

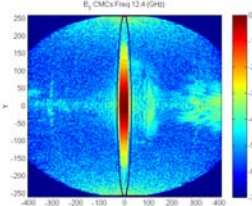


Figure 2 – CMCs after AUT translated to origin.

For the cases of spherical and cylindrical near-field measurements the highest order mode index is related to the MRE of the measurement. Thus as the AUT is displaced away from the origin of the measurement co-ordinate system the highest order mode index increases proportionally with the MRE. For the planar case, the origin of the measurement co-ordinate system is usually defined as being the centre of the aperture of the scanning probe when in the centre of the scan plan (this can be dependant upon the phase reference used during the auxiliary probe pattern calibration). Thus, for P-MARS it is the AUT-to-probe separation that is the *crucial* parameter, see Figure 3 below for a schematic representation of these parameters. Figure 2 above contains a false colour plot of the CMCs once the AUT has been mathematically translated back to the origin of the measurement co-ordinate system, *i.e.* the parabolic phase function that results from the finite non-zero AUT-to-probe separation has been removed from the far-field pattern. Here, it is clear that the CMCs associated with the AUT are confined to a narrow band that are tightly distributed about $n = 0$, *i.e.* in the centre of the plot with $|n| < 30$. As the total power radiated by the AUT must be conserved, the amount of power per mode must increase as the total number of modes associated with the AUT

decreases. As the amount of noise per mode can be seen to be roughly constant, in this case at circa -60 dB with respect to the maximum level, the effective system signal to noise (SNR) ratio of the measurement is increased.

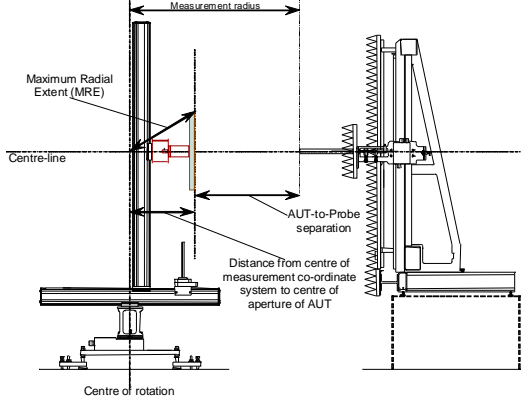


Figure 3 – Comparison of spherical, cylindrical and planar measurement geometries.

Crucially, and as has been observed previously with S- and C-MARS, although the AUT has been translated back to the origin of the measurement co-ordinate system, and as such can be represented with only a comparatively small number of modes, this is not the case for the scatterers which are spatially extended and are represented by higher order modes. In effect, the contributions in the domain of the CMCs from the AUT and the scatterers are separated, *i.e.* displaced so that they no-longer interfere with one another. This effect is clearly illustrated in Figure 2 where those modes associated with scatterers, *e.g.* $n = -300, 100, 250 - 400$, can be seen outside the $|n| = 30$ mode range which is represented with a black ellipse. Consequently, any mode that is of higher order than that required to reconstruct the field of the AUT can be filtered out using a band-pass brick-wall filter function as these modes can not be part of the antenna's far-field radiation pattern. Although the filtering is normally based on the MRE of the antenna, this may be increased for analysis purposes up to a limit determined by the dimensions of the planar near-field data set (*c.f.* for conventional spherical or cylindrical scanning this limit would be determined by the data point spacing). The mode filtered far-field pattern can be obtained by evaluating the inverse of equations 4 and 5,

$$E_A(r \rightarrow \infty, A, E) = -2k_0 \cos E \sum_{n=-\infty}^{\infty} (-j)^n B_n^1(\gamma) e^{jnA} \quad (6)$$

$$E_E(r \rightarrow \infty, A, E) = -2jk_0 \cos E \sum_{n=-\infty}^{\infty} (-j)^n B_n^2(\gamma) e^{jnA} \quad (7)$$

The mode filtering technique described above suppresses the effects of scattering principally in the xz -plane. However, scattering artefacts that have a component in the yz -plane, are essentially unaffected by this processing. Fortunately, it is a simple matter to repeat this processing once the filtered antenna pattern function has been rotated by 90° about the positive z -axis.

Thus, by implementing this processing in both horizontal and vertical axes, *all* of the range scattering effects can be very effectively suppressed.

3. Preliminary P-MARS Verification by Computational Electromagnetic Simulation

In order that the two-dimensional P-MARS processing algorithm could be verified, an x -band planar near-field measurement was simulated using two co-planar sources. Here, the sources were modelled as square apertures cut from an infinitely thin, perfectly electrical conducting (PEC) sheet that extends to infinity in each axis. The desired source was located symmetrically about the origin with the spurious secondary source/scatterer located at $x = y = -0.75$ m. By placing the secondary (spurious) source in the diagonal plane it insured that both x - and y -axis P-MARS suppression were verified. The far-field pattern was computed, tabulated on a regular azimuth over elevation co-ordinate system and resolved onto an azimuth over elevation polarisation basis using the usual near-field to far-field transform (no attempt was made to simulate probe pattern effects). This can be seen presented in Figure 4 in the form of a false-colour plot. Figure 5 contains the equivalent P-MARS filtered result. As can be seen, the high frequency angular ripple that results from constructive and destructive interference from the spurious source that is evident on the unfiltered plot is entirely absent from the P-MARS filtered plot.

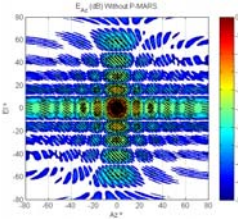


Figure 4 – Far-field pattern without P-MARS

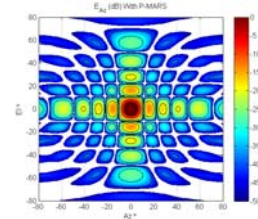


Figure 5 – Far-field pattern with P-MARS

Figure 6 and 7 contain comparisons of horizontal and vertical cardinal cuts. Blue traces denotes the ideal case, black traces denote P-MARS filtered results whilst magenta traces are equivalent multi-path levels (EMPL) [9]. Here, the greater the degree of agreement the smaller the EMPL which in this case can be seen to be below -70 dB level everywhere except for very large azimuth angles where minor differences are evident from interpolation.

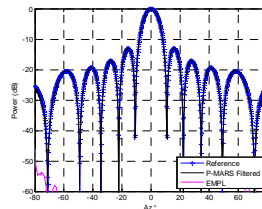


Figure 6 – H-cut comparison of reference & P-MARS

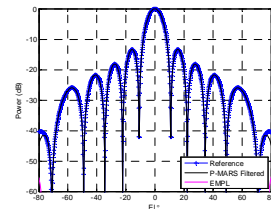


Figure 7 – V-cut comparison of reference & P-MARS

A number of other simulations were performed involving additional sources in various orientations all of which resulted in similarly encouraging results demonstrating the integrity of the underlying antenna pattern function after P-MARS processing. As these results were encouraging the research progressed to taking actual range measurements which are discussed in the following sections.

4. Preliminary P-MARS Verification by Range Measurement

Experimental verification of the P-MARS measurement technique was based upon assessing the repeatability between successive measurements where a single parametric change had been introduced. The intent being that the parametric change should be capable of being compensated for by P-MARS processing. Figure 14 shows an NSI-300V-12x12, 12'x12' planar near-field system installed within a partially absorber lined chamber. This system was used to acquire an NSI-RF-SG90 x-band standard gain horn (SGH).

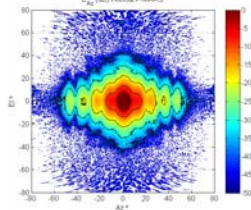


Figure 8 – Reference measurement

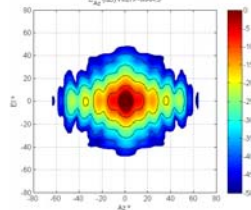


Figure 9 – Reference measurement with P-MARS

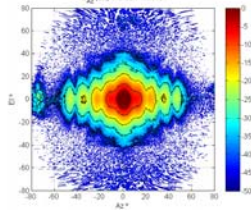


Figure 10 – Measurement with reflector on side wall

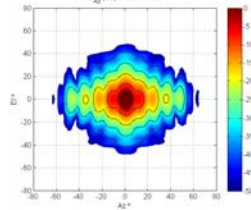


Figure 11 – Measurement with reflector and P-MARS

Here a baseline measurement was taken after which reflective aluminium foil was hung on the left hand wall of the chamber. This was intended to introduce a specular reflection into the antenna radiation pattern of the AUT. Figure 8 contains a false colour plot of the baseline SGH measurement. Here, some low level scatter can be seen at wide polar angles which manifests itself as high frequency ripple (speckle) at approximately the -30 dB level. Figure 10 contains the equivalent result showing the effect of the additional scatterer. Here, an additional spurious lobe can be seen at -70° to -80° in azimuth. Figure 9 contains the P-MARS filtered baseline pattern. From inspection it is clear that the underlying antenna pattern function has been preserved with the spurious multi-path having been attenuated. The P-MARS filtered measurement, Figure 11, with the reflector shows the

same antenna pattern function with the wide angle spectral flash having been attenuated together with general range multi-path. Figure 12 contains a comparison of the azimuth cardinal cuts of the baseline and reflector measurements. Here, the EMPL can be seen to show a general level of -60 dB over much of the forward half-space with that level increasing to just above -40 dB in the region of the spurious flash. Comparison with Figure 13 shows that the EMPL has been reduced to below -70 dB everywhere except near boresight where it rises to approximately -65 dB thus demonstrating excellent agreement between the respective results and a circa 10 to 15 dB improvement in agreement.

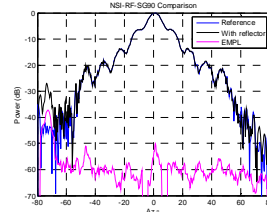


Figure 12 – Comparison of reference and reflector measurements

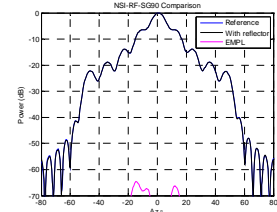


Figure 13 – Comparison of P-MARS processed reference and reflector measurements

Whilst this result is very encouraging, the measurement geometry meant that the reflection lobe was located at a comparatively low level and at a large pattern angle. Thus, in an attempt to contrive a far more demanding test, the reflecting foil was moved to the region of greatest field intensity and it was placed on the rear wall immediately behind the scan plane. This arrangement can be seen presented in Figure 15. Again, a reference measurement was taken followed by the scatterer contaminated measurement. Here, the measurements were taken at the lower end of the x-band so that the AUT pattern would be as broad as possible and so that effects over a larger proportion of the forward hemisphere could be examined.



Figure 14 – NSI-300V-12x12 system installed within a partially absorber lined chamber



Figure 15 – NSI-300V-12x12 shown with reflector placed behind scan plane

Figure 16 contains the far-field pattern of the scattering contaminated SGH measurement as obtained using conventional planar processing. Conversely, Figure 17 contains an equivalent plot of the same measured data after P-MARS processing has been applied. As before, the high frequency ripple has been effectively eradicated together with the spurious scattering that is clearly evident on the unfiltered results at $A = 25^\circ$, $E = -25^\circ$. Figure 18 contains a comparison of the azimuth cardinal

cuts prior to P-MARS processing. Conversely, Figure 19 contains an equivalent plot after P-MARS processing has been applied where it can be seen that the EMPL has decreased by more than 10 dB which is very encouraging.

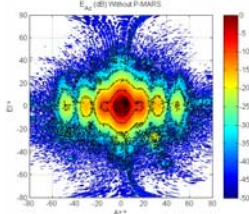


Figure 16 – Measurement with reflector on back wall

The slight rise in the EMPL for azimuth angles around 20° corresponds to the region where the scatterer had the greatest effect. However, the level is at circa -50 dB which is a good result.

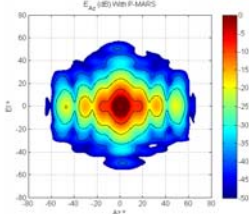


Figure 17 – Measurement with reflector and P-MARS

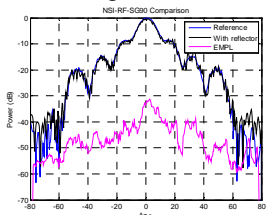


Figure 18 – Reference measurement versus measurement with reflector

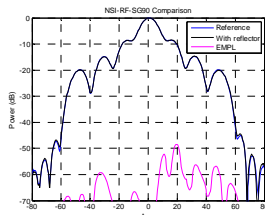


Figure 19 – P-MARS processed reference measurement and reflector measurements

An alternative multi-path suppression technique that has been known of for many years is the aperture plane spatial filtering technique [10]. This technique involves transforming a measurement back to the antenna aperture plane, using a conventional plane-to-plane transform [9]. This infinitely thin two-dimensional region of space would be chosen to be coincident and synonymous with the aperture plane of the AUT. All fields outside of the physical aperture of the antenna would be truncated, *i.e.* set to 0 V, whereupon the filtered far-field pattern would be calculated. Figure 20 and Figure 21 contain comparisons of the cardinal cuts of the unfiltered pattern, the P-MARS filtered pattern, and the aperture plane spatial filtered pattern. From inspection, it is clear that the P-MARS filtered measurement and the aperture plane filtered measurement are in encouraging agreement. However, it is worth noting the differences between the two filtering algorithms. The aperture plane filter technique requires the AUT to be an aperture type antenna. If the antenna does not have a well defined (*i.e.* tightly constrained *thin*) aperture then the effectiveness of the technique is far more limited. The SGH being characterised here is an aperture type antenna and as such constitutes an ideal candidate for this approach. However, even here, there are approximations. Any currents flowing on the exterior of the SGH will also radiate and contribute to the true far-field pattern and these too will be removed from the filtered far-field pattern thereby introducing an additional inaccuracy. P-

MARS does not impose such an aggressive filter as it effectively removes fields outside a three-dimensional region of space that encloses the AUT. Thus, its success does not depend upon the AUT being an aperture type antenna and, for example, would be equally effective for the case of a “thick” antenna, *e.g.* a log periodic dipole array antenna. External currents such as those flowing down the outside of a SGH, *etc.*, are also not removed from the P-MARS filtered far-field pattern.

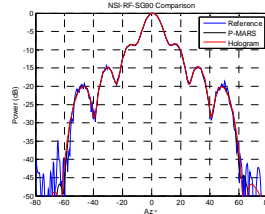


Figure 20 – Comparison of azimuth cardinal cuts

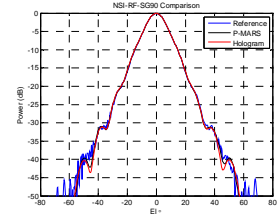


Figure 21 – Comparison of elevation cardinal cuts

MARS processing has been successfully deployed for spherical, cylindrical, and now planar geometries. The NSI-300V-12x12 system also comprised cylindrical and spherical upgrades providing the opportunity to perform an intra-geometry comparison. Thus, the SGH was acquired using each geometry and the resulting data was transformed to the far-field with and without MARS processing. From inspection of Figure 22 and 23 it is clear that the degree of agreement has significantly improved with MARS processing, particularly at wider angles. The far wide out sidelobe structure that was hitherto obscured by multi-path subsequently becoming clearly revealed with MARS processing.

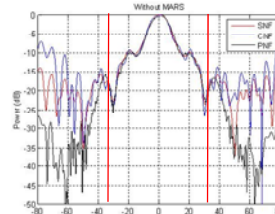


Figure 22 – Without MARS processing

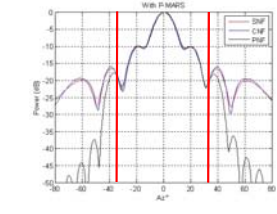


Figure 23 – With MARS processing

Unfortunately, due to the requirement to prevent mechanical interference, the AUT-to-probe separation was larger than is ideal for a planar near-field measurement resulting in the onset of the first order truncation effect at a little more than 30° away from boresight. This is illustrated in the figures with vertical red lines. It is crucial when reviewing these results to recognise that almost everything is different between planar, cylindrical and spherical measurements and transformations and that the differences shown above contain not only difference resulting from multi-path but additionally the respective uncertainties associated with each of the individual measurement systems.

The detection and conversion of the RF signals to real and imaginary, or amplitude and phase, components in

receivers can introduce a small bias error that can produce a very small constant signal on the recorded amplitude and phases of the near-field pattern. This signal may be as much as 50 to 100 dB below the peak near-field amplitude, but in the FFT processing of the data for planar measurements, the leakage signal is summed coherently in the on-axis direction which can produce a noticeable distortion in the main beam region if the measurement area is much larger than the AUT area. As the P-MARS processing technique essentially limits the far-field pattern to contributions from within a certain user controlled three-dimensional region of space that bounds the AUT errors like this are greatly suppressed. This is illustrated in the following results. Figure 24 and 25 present the far-field pattern of an x -band SGH where a receiver bias is present in the near-field data. The effect of this is clearly visible on the far-field cross-polar pattern where a spurious spike is present on axis (-30 dB at $A = E = 0^\circ$).

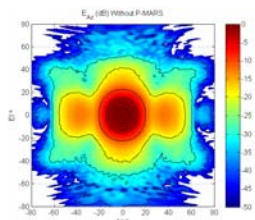


Figure 24 – Copolar pattern

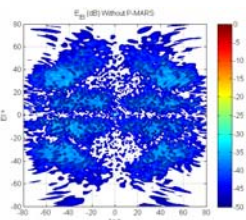


Figure 25 – Cross-polar pattern

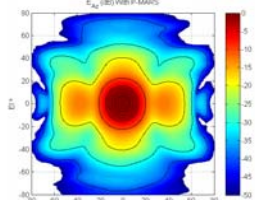


Figure 26 – Copolar pattern with P-MARS

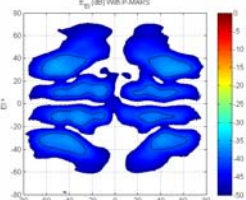


Figure 27 – Cross-polar pattern with P-MARS

Figure 26 and Figure 27 contain the P-MARS filtered far-field copolar and cross-polar patterns. Here, as expected, chamber multi-path can be seen to have been suppressed. However, the receiver bias error has also been suppressed. Whilst techniques for compensating for this error are well known [11], P-MARS processing constitutes a highly effective alternative.

5. Summary And Conclusions

Planar, cylindrical and spherical MARS processing can be used with a very high degree of confidence since all the steps in the measurement and analysis are consistent with the well established principles of the standard near-field theory and measurement technique, and all comparisons to date have proved *overwhelmingly* positive. The offset of the AUT and the resulting smaller data point spacing are valid if the spacing satisfies the sampling criteria. The translation of the far-field pattern to the origin with the application of a differential phase

shift is rigorous. The selection of the mode cut-off for the translated pattern is based on the physical dimensions of the AUT and its translated location. The results of the planar, cylindrical and spherical MARS processing will reduce, but not entirely eliminate, the effect of the scattering. The final result with MARS processing can be degraded if the sampling of the near-field data is too coarse, or the mode filter is too tight, *i.e.* abrupt, but this is also true for regular planar, cylindrical and spherical processing. Importantly, both of these parameters are controlled by the user and must be correctly specified. As has been demonstrated, these frequency domain measurement and processing techniques are quite general and can be used to achieve acceptable results with use of minimal absorber or even without the use of an anechoic chamber. It can also improve the reflection levels in a traditional anechoic chamber allowing improved accuracy as well as offering the ability to use existing chambers down to lower frequencies than the absorber might otherwise indicate. Crucially, and for the first time, this paper has demonstrated the successful application of the MARS principle in a planar near-field antenna measurement facility.

6. REFERENCES

- [1] A.C. Newell, "Error Analysis Techniques for Planar Near-field Measurements", IEEE Transactions on Antennas and Propagation, vol. AP-36, pp. 754-768, June 1988.
- [2] E.B. Joy, "Near-Field Range Qualification Methodology", IEEE Transactions on Antennas and Propagation, vol. AP-36, pp. 836-844, June 1988.
- [3] G.E. Hindman, A.C. Newell, "Reflection Suppression in a large spherical near-field range", AMTA 27th Annual Meeting & Symposium, Newport, RI, October. 2005.
- [4] G.E. Hindman, A.C. Newell, "Reflection Suppression To Improve Anechoic Chamber Performance", AMTA Europe 2006, Munich, Germany, March 2006.
- [5] S.F. Gregson, A.C. Newell, G.E. Hindman, "Reflection Suppression In Cylindrical Near-Field Antenna Measurement Systems – Cylindrical MARS", AMTA 31st Annual Meeting & Symposium, Salt Lake City, UT, November 2009.
- [6] S.F. Gregson, A.C. Newell, G.E. Hindman, M.J. Carey, "Advances in Cylindrical Mathematical Absorber Reflection Suppression", 4th European Conference on Antennas and Propagation, Barcelona, 12th - 16th April, 2010.
- [7] D.M. Kerns, "Plane-Wave Scattering-Matrix Theory Of Antennas And Antenna-Antenna Interactions", Nat. Bur. Stand. (U.S.) Monograph 162, June 1981.
- [8] C. Cappellin, A. Frandsen, O. Breinbjerg, "On The Relationship Between The Spherical Wave Expansion And The Plane Wave Expansion For Antenna Diagnostics", AMTA Europe Symposium, Munich, Germany, 2006.
- [9] S.F. Gregson, J. McCormick, C.G. Parini, "Principles of Planar Near-Field Antenna Measurements", The Institution of Engineering and Technology, UK, 2007.
- [10] F.J. Cano-Fácila, M. Sierra-Castañer, J.L. Besada, "New Applications of Diagnostic Techniques In Antenna Measurements", AMTA Proceedings, Salt Lake City, November, 2009.
- [11] Rousseau, P. R., "An Algorithm To Reduce Errors In Planar Near-Field Measurement Data, AMTA Proceedings, October 1999.